The Time of Flight Upgrade for CLAS at 12GeV

by

Lewis P. Graham

Bachelor of Science
Benedict College, 2002

Submitted in Partial Fulfillment of the Requirements
for the Degree of Master of Science in Physics
College of Arts & Sciences
University of South Carolina
2008

---	---
Director of Thesis	2nd Reader
---	---
3rd Reader	Dean of The Graduate School

ACKNOWLEDGMENTS

I thank Professor Ralf Gothe for his help and guidance during this time we have worked together. His philosophy and approach to physics and research has inspired me to understand every problem, exhaust every possible solution, and optimize the appropriate conclusion to extend to all aspects of physics. He is a great professor and mentor.

I thank Dr. Kijun Park for his extremely valuable feedback and suggestions.

I thank all my colleagues who helped me working on this study: Collin Eaker, Dominik Gothe, Evan Phelps, Haiyun Lu, Legna Torres, and Zhiwen Zhao.

I thank my family P, Mary, Alicia, and Tara for their patience and support.

ABSTRACT

The Time of Flight (TOF) system is a detection system within the CEBAF Large Acceptance Spectrometer (CLAS) at Thomas Jefferson National Accelerator Facility. CLAS, being a multi-gap toroidal magnetic spectrometer, is used in the detection of particles and their varying properties and interactions. The Thomas Jefferson National Accelerator Facility provides a continuous electron beam of energy 6GeV, to investigate nuclear reactions by obtaining the identification and energy of the production particles. The CLAS detector is designed and currently runs at energies of up to 6GeV, but with recent approval it will be upgraded to energies of 12GeV. CLAS consists of drift chambers to determine the charged particle paths, gas Cherenkov counters for electron discrimination, TOF scintillators for nucleon and meson identification, and an electromagnetic calorimeter for identifying showering electrons and photons. The TOF system, which is our focus, is composed of scintillation counters at the forward angle, and covers an area of 206 meters squared. Therefore, we look to upgrade and construct the TOF system of CLAS and outline strategies of current construction, purpose for design, and outlook for the Forward TOF system upgrade. First results have led to the conclusion that of two timing methods performed, the Source Method will produce better time resolution results after further optimization.

LIST OF FIGURES

TABLE OF CONTENTS

1) INTRODUCTION

The thrust of modern experiment embodies the study of the nucleon through exclusive and semi-exclusive processes to provide new insights into nucleon dynamics down to the elementary quark and gluon level. Through inclusive scattering of high-energy leptons off the nucleon, primary investigations into the internal structure of the nucleon have been performed for many years. These inclusive measurements are insensitive to the internal quark-gluon dynamics; furthermore they provide a one-dimensional image of the quark longitudinal momentum distribution. With these inclusive measurements at current availability, the demand to date is for various exclusive measurements into nucleon dynamics. Thus, the precedent for the CLAS 12 GeV upgrade is valid, and needed to move the study of the internal nucleon dynamics to the next level.

The CLAS 12 detector is an evolution of the present CLAS to meet the demands for advance studies into the structure of nuclei. The upgrade will be required to provide access to generalized parton distributions in exclusive reactions. To adequately foster these needs, CLAS 12 will need to accommodate a higher energy, and a higher luminosity continuous electron beam. The two major components of the upgrade are the existing Forward Detector and a new Central Detector to be installed around the target. Thus, our present agenda is to focus

our work on the Forward Detector portion. The Forward Detector detects neutral and charged particles from angles of 5° up to 40°. Presently, it consists of 7 main sub-detectors for the precise detection of particles.

Figure 1.1 shows the present CLAS detector and all the components. The first important feature of the Forward Detector is a toroidal magnet to produce an azimuthally symmetric field. The toroidal magnet does not really serve as a unit of detection but more a device for manipulating particle trajectories and paths according to their momenta. The first components of the Forward Detector are drift chambers (DC), used to acquire the trajectories of charged particles. Cerenkov Counters (CC) make up the second component housed in the Forward Detector. They are used to discriminate electrons from all production particles of the various reactions. The third component, Scintillation Counters (SC), determine the time of flight for particles traveling from the target to the detector. After the scintillation counters comes the Electromagnetic Calorimeters (EC) which are used in detecting showering particles. These make up the fourth component of the detector. The next important feature would be the two-level trigger system contained by the Forward Detector. This system initiates data conversion and fast readout. The Data Acquisition (DAQ) is the final important feature of the detector where it collects all digitized data and stores it for later analysis. Amongst the 4 components that make up the Forward Detector, the TOF system inherits our focus for the upgrade of CLAS at 12GeV.

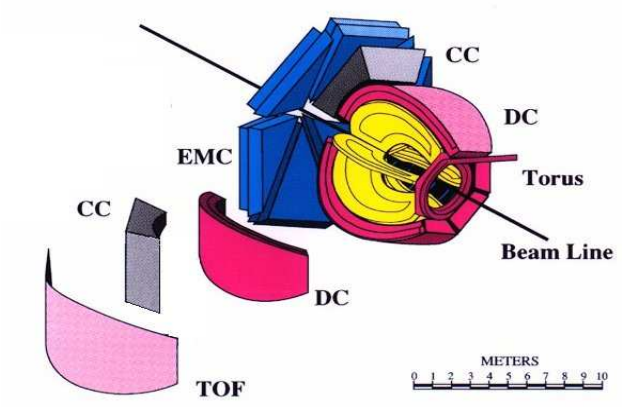

Figure 1.1: CLAS Detector[1].

The Time of Flight (TOF) system is designed to decipher the flight time of particles produced from incident radiation reactions. If a particle's start position and momentum are known by taking the path length information to where it was detected in TOF, one can calculate the velocity of that particular particle. The time of flight system at CLAS uses the start time arrival time of a particle to govern its flight time. The system was purposed to include good timing resolution to adequately identify particles and also obtain good segmentation to provide flexible triggering and pre-scaling. The time of flight system is subdivided into two groups which are parameterized by the scattering angle of the reaction particle. At angles of 0° to 40°, TOF is comprised of what are known as the small (forward) angle counters. At these angles, the scattering angle is minimal and the particle inherits more momentum. From 41° and above, these are known as

[1] The Diagram show the different components that make up the CLAS detector.

the large angle counters. One important advantage of the reconstructed angles is depending on the orientation of the magnetic field, the bending angle provides immediate information as to the charge of particles within the reaction. The TOF system is equipped for a resolution of σ = 120ps at the smallest angles and 250ps at angles of 90° and larger. These specifications are required by the fact that at small angles, the most energetic particles are produced requiring a better resolution where this lessens with each increment in the angle. Using off-line analysis, the identification of particles is achieved by correcting leading-edge discriminator based time measurements with pulse-height information for the introduced time-walk. Thus, the system is required to give signals that represent a uniform response to selected particles that reach the time of flight detectors. The TOF system is not only used to determine the particles' velocity but can also be used for energy-loss measurements. Energy loss in the counter is proportional to pulse-height information which means there is a separate way to identify slow particles. If multiple scattering particles dominate the tracking resolution, then the particle's distinct energy loss can also give a better measurement of particle energy. In addition to excellent timing resolution and segmentation, the TOF system has to be able to operate in a high-rate environment. Being that all detectors must be optimized for best results, the time of flight system for CLAS is one of several detector subsystems being upgraded to unveil new and exciting physics. For this reason, we have taken on the challenge and lead in prototyping and eventually building the new time of flight system that will operate at 11GeV.

CHAPTER 2: DESIGN OF TOF SYSTEM

2.1) SCINTILLATION MATERIAL

The most important and vital component within the detection system is the scintillation material. The scintillator provides a small flash of light or "scintillation" when struck by a particle or nuclear radiation. Radiation passing through the scintillator bar excites the molecules that make up the material. The excitation comes on absorbing the energy from the incident radiation, where the scintillator undergoes excitation to a higher electron state followed by a prompt or delayed return to the ground state. Once these molecules are excited, then light is emitted and propagates through the scintillation material. This light is then converted into a current of photoelectrons by a photomultiplier tube (PMT), where the current signal is enhanced providing easier detection.

In our prototype testing Bicron BC-408 plastic scintillators, which are currently used in the existing time of flight detector at Jefferson Lab, were used in the time resolution measurement. The basic premise of our method is to first reproduce the time resolution gained in the previous prototype for CLAS at 6 GeV. Reproducing this resolution or obtaining a better value would give us validable consistency in our setup and electronics. Thus changing additional hardware such as scintillation material and PMTs will help improve the timing resolution.

Scintillators are excellent testing material because of the information their signal can provide. They are extremely sensitive to energy, in that the light output is directly proportional to the energy loss.

Scintillation detectors have a fast timing response and recovery rate. The fast response allows superior accuracy in the collected timing information, and the quick recovery allows more data to be taken due to less time being demanded between events. The advantages of using a plastic scintillator are numerous. They provide extremely fast signals and an immense light output. The plastic bars are easily mechanized because they are flexible under the right amount of pressure. This is key in the setup because it provides connectivity options to either light guides or directly to the photomultiplier tubes (PMT) for greater precision.

2.2) PHOTOMULTIPLIER TUBES

In nuclear and high-energy physics, PMTs are widely used in scintillation detectors. PMTs are electron tube devices which convert light into an electric current that can be measured. They consist of a photocathode made of sensitive material for photon-electron conversion. The photocathode is followed by a collection and multiplication system for electrons. The photocathode consists of a material with a low work function, simply meaning its ionization energy is low enough for visible or ultra-violet photon energies to create a free electron and give enough kinetic energy to escape from the surface region. From the

scintillator, an incident photon impinges upon the photocathode which produces the emission of an electron by the photoelectric effect. The applied voltage then directs and accelerates the electron to the first dynode. Secondary electrons are emitted from this dynode and directed and accelerated to the next dynode, and so on this process continues creating a shower of electrons. The anode collects this cascade of electrons which produces a typical analog current of 40mA for further measurement and testing in the electronic chain. After amplification through the multiplier structure, a typical scintillation pulse will give rise to $2.5X10^{10}$ electrons, sufficient to easily serve as the charge signal for the original scintillation event. Figure 2.1 shows the schematics of a PMT and how the incident photon produces the electron avalanche passing through the dynode layers.

The XP2020/UR PMTs were chosen in our prototype experiment. These tubes possess a faster rise time over the existing tubes used in the CLAS detector today.

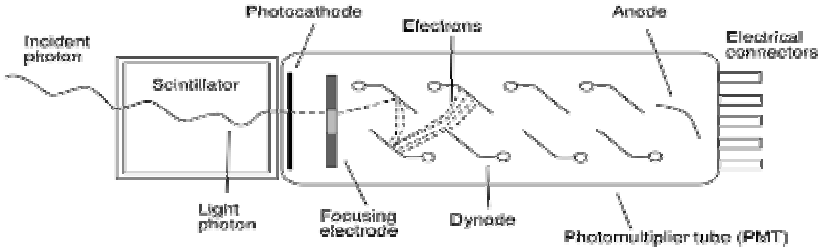

Figure 2.1: Schematic of the photon process as light propagates through scintillation into the photomultiplier tube and through the various components of the tube [2].

Once a signal is passed through the PMT diagram, it can be taken from two points, the anode and the last dynode. The anode signal is larger than the dynode signal since it is multiplied by one more stage. The anode signal will be used for triggering, while the dynode is used for measuring the amplitude signal.

2.3) VOLTAGE DIVIDERS

Dividers use high-voltage field effect transistors to fix the PMT gain by stabilizing the voltage even at high signal rates, and to protect the PMT against too high light levels where they would shut down the circuit if such an over-current would occur. We utilized VD127K [8] voltage dividers in our measurements.

[2] Diagram displays scintillation counter attached to photomultiplier tube and the process a photon goes through once it reaches the tube.

2.4) LIGHT GUIDES

A light guide plays the role of mediator between the scintillation material and the photomultiplier tube. Light guides are used to connect the scintillators to the PMTs to optimize the light transmission. For various reasons, such as oddly shape scintillation or magnetic field presence, light guides may be needed. The light guide provides transmission by relying on total internal reflection of the light signal through its internal walls from one end to the other. For our purpose, a light guide for the shape adaptation between the PMT and scintillation bar is not needed. In our prototyping, we had simulation done to take into account the loss due to reflections at the interfaces of the glass envelope of the phototube to the light guide and the light guide to the scintillator. In Figure 2.2, the ratio in percentage is shown of the light that has entered the light guide to the amount that enters the glass envelope of the PMT.

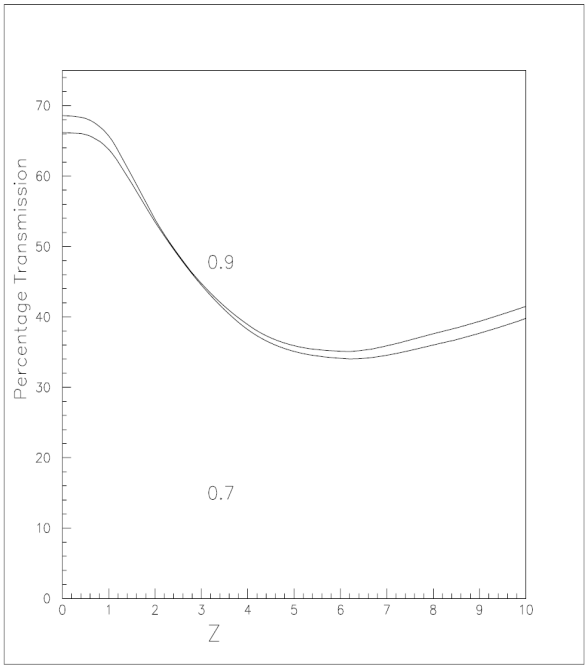

Figure 2.2: Simulated results of light transmission (%) into photomultiplier tube with respect to light guide length[3].

As we see in Fig. 2.2, light transmission versus the length of the tube where z=0 would be the tube directly connected to the light guide. The 70% represents aluminized mylar film and the 90% is for 3M plastic foil. From the simulations, we see that we increase light transmission into the glass envelope of the PMT directly attaching the PMT to the scintillation. This will be one of the setups that we test along with different geometrical shaped light guides.

[3] Diagram displays the percentage of light that would be transmitted into the glass envelope of the photomultiplier tube with respect to having a light guide attached. The z axis represents the length of the light guide, where z=0 would be no light guide.

CHAPTER 3: ELECTRONICS

Nearly all nuclear and particle physics experiments today utilize data acquisition systems that are controlled or monitored by computers. These computer controlled systems are for the most part the mandate of modern measurements and experimentation in nuclear physics. These mandates vary from the significant amount of data needed to be processed by a fast, capable system to the necessity of efficient validating by results from studies. The processing system used in our experiments and testing is a Computer Automated Measurement and Control system (CAMAC). This system acts as an interface between the equipment utilized in the lab and the computer. A CAMAC "crate" as it is known, physically consists of about 20 slots or stations for plug-in module instrumentation. The system also has a controller module that allows each individual module to be operated and controlled by an external computer through an interface application.

The primary application of the CAMAC system is data acquisition, but it may also be used for remotely programmable trigger and logic applications. The major advantage of the housed module instrumentation in the CAMAC is the ease it provides through the Global Positioning Interface Board (GPIB), and the speed it has in local data manipulation. Its function is to provide a scheme to allow a wide

range of modular instruments to be interfaced to a standardized backplane called a DATAWAY. Within the crate, each connector provides access to the dataway, which is a data highway consisting of conductor busses for digital data, control signals, and power. Module and CAMAC communication takes place through the DATAWAY control of the CAMAC system. Through the DATAWAY, commands and data are transferred between system, modules, and controller. Thus, the system standard precisely covers the electrical and physical specifications for the modules in use, instrument housings or crates, and a crate backplane. In this way, additions to a data acquisition and control system may be made by plugging in additional modules and making suitable software changes. Thus, CAMAC allows information to be transferred into and out of the instrument modules.

The CAMAC in our case helps to interpret the signals outputted from the photomultiplier and sends this information to the computer in an understandable format. It correlates these signals but also measures the signal strength which gives the charge that the PMT delivered, telling us the overall gain.

For radiation detector applications operated in pulse mode, the detector output has to be converted to a linear pulse where the shape and amplitude will carry information of the experiment. Prior to being recorded, this linear pulse may be administered in the signal chain or converted into a logic pulse to obtain other information. In the signal chain, an assortment of electronic units are used to perform a wide range of functions from providing a linear pulse output to the CAMAC system, to converting the linear pulse to a logic pulse for further analysis.

The primary application of the CAMAC system is data acquisition, but it may also be used for remotely programmable trigger and logic applications. The major advantage of the housed module instrumentation in the CAMAC is the ease it provides through the Global Positioning Interface Board (GPIB), and the speed it has in local data manipulation. Its function is to provide a scheme to allow a wide range of modular instruments to be interfaced to a standardized backplane called a DATAWAY. Within the crate, each connector provides access to the dataway, which is a data highway consisting of conductor busses for digital data, control signals, and power. Module and CAMAC communication takes place through the DATAWAY control of the CAMAC system. Through the DATAWAY, commands and data are transferred between system, modules, and controller. Thus, the system standard precisely covers the electrical and physical specifications for the modules in use, instrument housings or crates, and a crate backplane. In this way, additions to a data acquisition and control system may be made by plugging in additional modules and making suitable software changes. Thus, CAMAC allows information to be transferred into and out of the instrument modules.

The CAMAC in our case helps to interpret the signals outputted from the photomultiplier and sends this information to the computer in an understandable format. It correlates these signals but also measures the signal strength which gives the charge by the PMT delivered, telling us the overall gain.

For radiation detector applications operated in pulse mode, the detector output has to be converted to a linear pulse where the shape and amplitude will carry information of the experiment. Prior to being recorded, this linear pulse may be

administered in the signal chain or converted into a logic pulse to obtain other information. In the signal chain, an assortment of electronic units are used to perform a wide range of functions from providing a linear pulse output to the CAMAC system, to converting the linear pulse to a logic pulse for further analysis.

3.1) INTEGRAL DISCRIMINATOR

The first module used in the signal chain is a leading edge discriminator, where its function is to convert an analog signal into a logic signal. A linear pulse enters the discriminator which is set to a pre-determined threshold. Once the input amplitude exceeds the set discrimination level, it is converted into a logic pulse. As alluded to by ***Knoll G., 1979*** [5], "In order to count the pulses properly, the linear pulses must be converted into logic pulses." The discriminator is the simplest unit which can be used for this conversion. After the "leading edge" of the linear pulse crosses the discrimination limit, a logic signal is produced to count and time the linear pulses. This is known as "leading edge timing" and is the basic timing we used for our measurements. The key to maximizing measurements with this module is to set the threshold level just above the system noise. In so doing, we maximize its sensitivity for counting detector pulses of all sizes to ultimately enhance the signal-to-background counting ratio. According to ***Knoll G., 1979*** [5], "The stability and linearity of the discriminated adjustment are usually adequate for routine applications but may become important specifications for demanding situations." Simply, the discriminator reads a signal and decides if it is strong enough to be the actual signal or if it is

simply noise. If it is determined to be strong enough and above the set threshold, then the signal is passed to the next component in the signal chain.

3.2) SCALER

For adequate counting procedures in the measurement, the logic pulses must be accumulated and the total number recorded over a fixed interval of time. The scaler performs this process where a simple digital register is incremented by one count each time a logic pulse is received as an input. Scalers are typically operated in one of two modes: preset time and preset count. The counting period is controlled by an external timer in the preset time mode. In the preset count mode, pulses are accumulated until a certain amount is achieved thus ending the counting interval. This latter method was used in our resolution measurements and will be explained in detail in the resolution chapter. Overall, the scaler simply counts the number of signals it receives for a set time period, a set maximum count, or until it is manually stopped.

3.3) COINCIDENCE

For coincidence systems, one of the signals serves as a “gate” for the other incoming signal. The gating pulse must be shaped to define exactly its start and end time. ***Eichholz G., 1979*** [3] states that the second signal may contain information on the initiating particle and functions to pass the gate if it arrives during the appropriate interval without undergoing any shaping itself. The

overall purpose of the coincidence system is to distinguish signal from background events. The principle interest for coincidence circuits is the simultaneity of events recorded by different detectors or traveling along different electronic pathways. The need therefore arises to have these separated events correlate for a common purpose in the electronic chain. Two events are said to be simultaneous if the interval between them is too short for them to be distinguishable. Events are rejected or seen as not simultaneous if their time of separation exceeds the resolving time of the circuit.

The coincidence functions to accept logic pulses of two or more inputs. The module is defined by the user to accept pulses within the given time interval, and when a preset number of input pulses are received during this time interval then a single logic pulse is outputted and passed on to the next component.

3.4) TIME-to-DIGITAL CONVERTER

A time-to-digital converter is a circuit that can convert a time interval between two pulses (usually digital signals) directly into a digital number proportional to that time interval. The simplest method of achieving this utilizes a high frequency oscillator. The oscillator is then started and stopped by the pulses, and the time resolution is then confined by the frequency of the oscillator.

To obtain a digital time interval measurement, the most direct method is to utilize the stable oscillators and counting methods. The module that performs this logic function is known as a time-to-digital converter (TDC). The basic concept of this method is that a digital signal coming from the coincidence module acts as a START signal for the TDC module to begin counting a constant frequency oscillator or more simply to start a clock. A second signal, that is appropriately delayed, coming from a discriminator logic unit serves as a STOP signal and a counting value is produced which is directly proportional to the time interval being recorded.

Once a STOP is received, the scaler and timer both are gated off, and the readout system is triggered by an interrupt signal. After the readout is successful, it generates a CLEAR signal to the timer window and the scaler. The system then awaits another event to carry out the process again. The timing system for a TDC module is completely adequate in timing efficiency for resolution testing. Not only does it hold these set parameters for processing an event, but it contains likewise signal generation to CLEAR and re-START the TDC, scaler, and timing window units upon a hang up or block in the system during measurement.

3.5) ANALOG-to-DIGITAL CONVERTER

The analog-to-digital converter (ADC) is responsible for converting all analog signal information into a digital form. The function of the ADC is to derive

a digital number that is proportional to the integral of the input signal. The resolution of the ADC depends on the range of digitization, in that, the higher the digitization capability of the module, the greater the resolution obtained.

The performance of the ADC is characterized by several parameters. The first, being its linearity of the conversion. Simply stated, the consistency in the digital signal is directly proportional to the integral of the input signal. Thus the ADC can provide direct information as to the energy distribution of the radiation source or the energy loss of a charged particle passing through the scintillator. (An advantage of the ADC unit is having one to one correspondence in the energy to signal integral.) Thus an important aspect is to monitor and test the linearity of the module. The second parameter would be the conversion speed from analog to digital information. In this instance our purpose and experimental setups demand fast measurement; therefore the ADC must contain a high or relatively adequate conversion rate sufficient for fast measuring.

CHAPTER 4: MU-METAL SHIELDING TESTS

In the Forward TOF PMTs face a separate obstacle in addition to operating for high volume rates with an adequate efficiency. They must also resist the influence of stray magnetic fields which come from the torus magnet. To protect the phototubes from these field strengths, magnetic shielding must be incorporated into the overall design of the TOF system. In our prototype, we performed tests using the existing mu-metal shielding geometry and thickness for CLAS. The shielding must protect the PMT from dominantly axial fields but also from transverse magnetic field components. ***Smith E., 1999*** [6], cites that the TOF scintillation counters are presently about 5m from the area of the target and in a local field of less than 10G. So our purpose was to test mu-metal shielding at different magnetic field strengths for PMTs.

We had a cylindrical mu-metal geometry fabricated with a thickness of 1mm to match the existing shielding at CLAS.

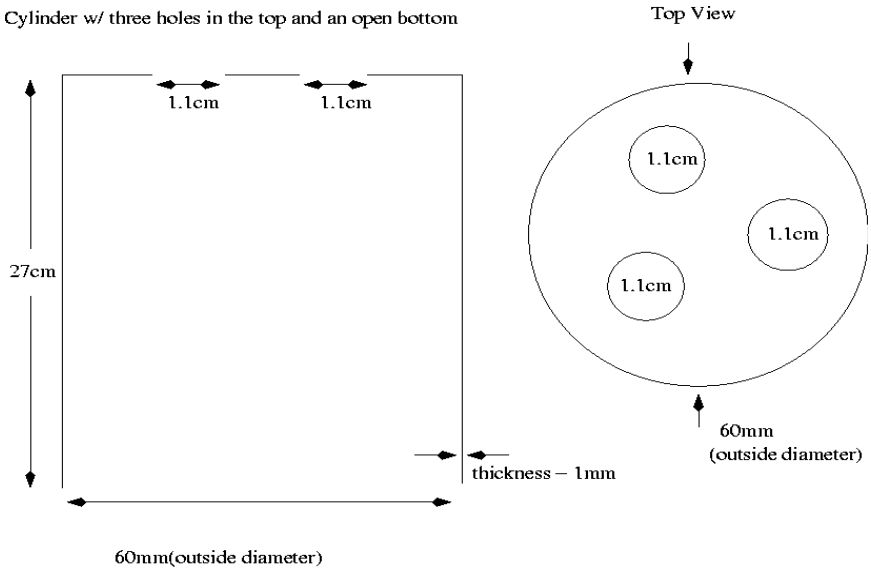

Figure 4.1: Schematic of Cylindrical mu-metal fabrication [4].

With this shielding, we had an end cap to improve the shielding of the axial component of the field. Fig. 4.2 shows the results from our measurements.

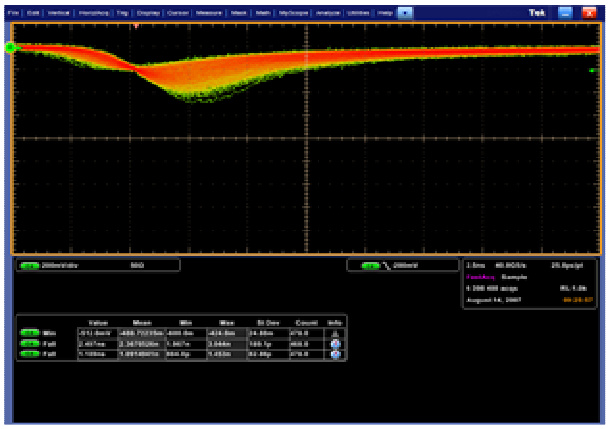

[4] Diagram displays the two-dimensional view and dimension of the cylindrical mu-metal fabrication with sealed end cap.

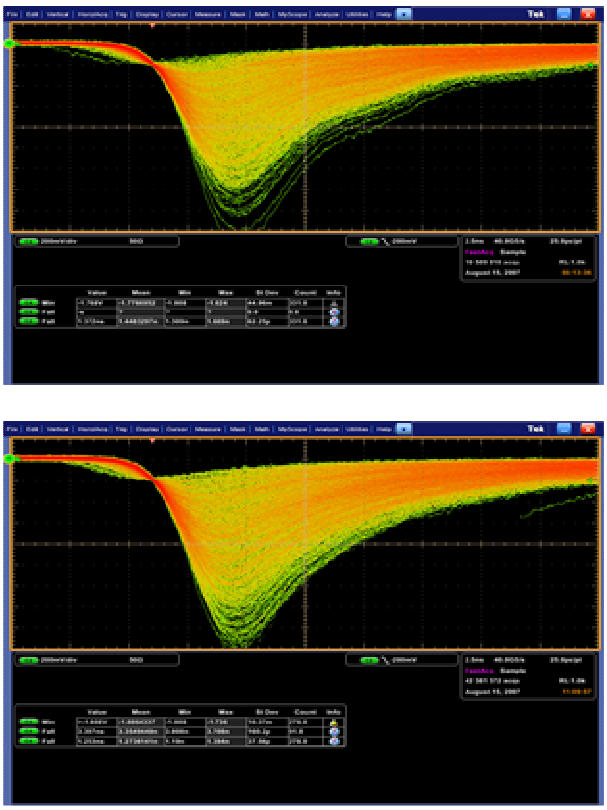

Figure 4.2: Images of Signal amplitude with respect to magnetic shielding[5].

From the images, we found that the amplitude of the signal is greatly affected without using any shielding for the PMTs. With shielding the axial field's influence on the amplitude of the signal is greatly reduced, and with an end cap even more. Our study of the mu-metal shielding has solidified the belief that the PMTs must have shielding because of the negative influence of the magnetic

[5] First image shows affect of magnetic field on signal amplitude with no shielding on PMT. Second image shows affect with shielding but no end cap. The third image shows magnetic field effect with shielding and end cap.

field. Also, it has given us new ideas in how to adequately accomplish this goal with an optimal design. For future measurements, we have designed a square cross section of mu-metal with a sealed end cap.

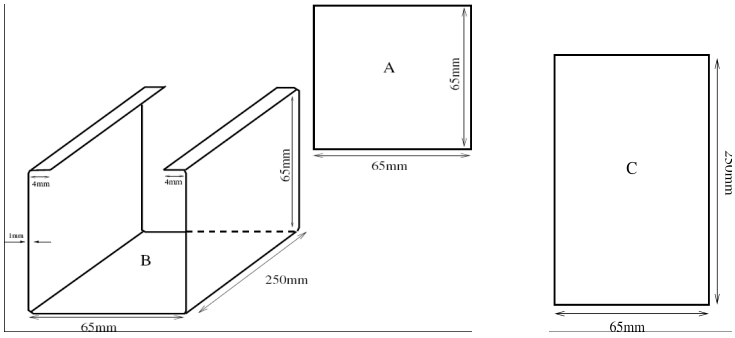

Figure 4.3: Schematic of Square mu-metal fabrication [6].

This geometry will allow us to stack square pieces of 1mm thickness onto the shielding to test the best thickness for optimal shielding, more so to allow flexible additions in the stacking region where the PMTs are staggered.

[6] Diagram displays the three-dimensional view and dimensions of the square mu-metal fabrication with sealed end cap for future testing.

CHAPTER 5: CABLE DELAY & RISE TIME TESTS

The consistency of the electronic chain is vital to all measurements performed for prototyping. In several timing applications and measurements, the need will arise to utilize delays at some instance of the electronic chain of the signal production. These delays are generally needed to adjust timing mandates or simply to perform calibration. For delay gain, coaxial cables are used to connect the various modules providing a desired transit time of the logic signal along the electronic chain. Since many of our operations required additional delay, we performed a series of measurements on various coaxial delay cables to test their efficiency and capabilities.

The first measurement we carried out was the attenuation through the cable delays. Five separate types of coaxial cable, RG-58, RG-214, RG-8, RG-9913, and RG-174, were used in this test. The method consisted of running a periodic signal through a leading-edge discriminator (LED), and the cable in testing. Then the signal was outputted to an oscilloscope for analysis.

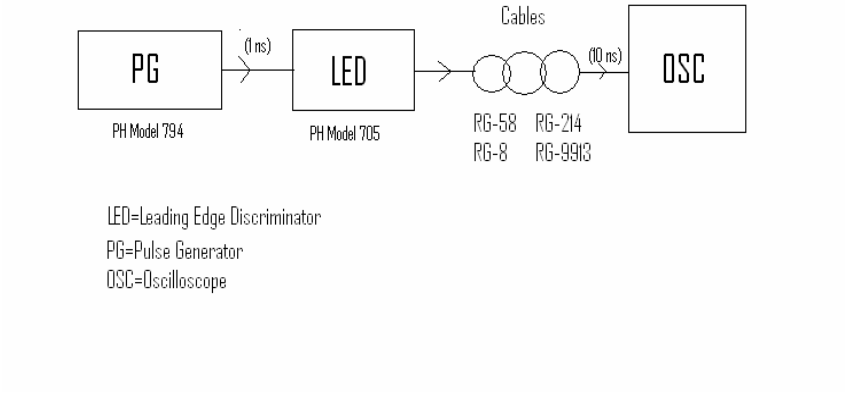

Figure 5.1: Cable Attenuation Schematic[7].

Cable Type	Cable Length	Delay Time	Signal Speed	Amplitude	Rise Time (30% to 70%)	Rise Time (10% to 90%)	Oscilloscope Image
RG-9913	251.5 ft.	303.7 ns	25.24 cm/ns	1.4 V	1.78 ns	10.55 ns	RG-9913
RG-8	202.2 ft.	310.6 ns	19.84 cm/ns	1.432 V	2.69 ns	12.69 ns	RG-8
RG-174	128.2 ft.	198.35 ns	19.7 cm/ns	1.072 V	4.30 ns	18.03 ns	RG-174
RG-214	95.3 ft.	147.4 ns	19.71 cm/ns	1.464 V	1.36 ns	7.01 ns	RG-214
RG-58	200 ft.	323.3 ns	18.86 cm/ns	1.32 V	5.67 ns	22.04 ns	RG-58
None	-	-	-	1.52 V	.836 ns	2.37 ns	Direct Input

Figure 5.2: Table of Measured Cable results[8].

[7] The Diagram shows a Philips (PH) pulse generator (PG) generating random pulses into a leading edge discriminator (LED) through different cables to be tested, RG-58, RG-8, RG-9913 and RG-214 into the oscilloscope (OSC).

The rise time for each signal was measured for 10%-90% and 30%-70% of the leading edge of the signal.

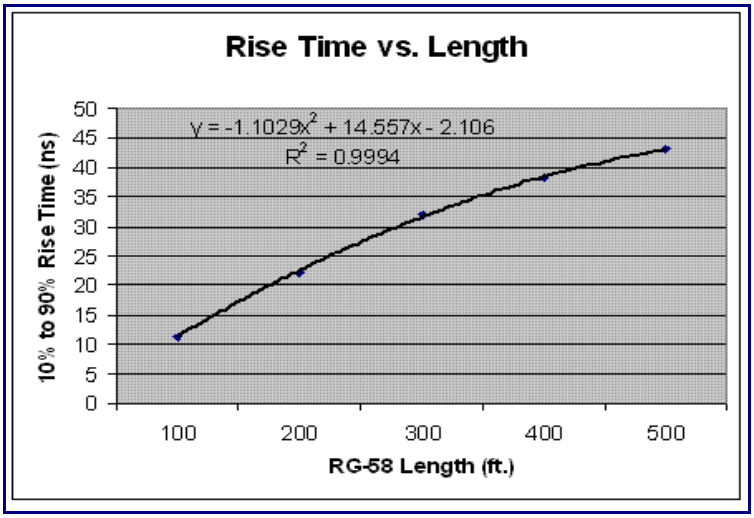

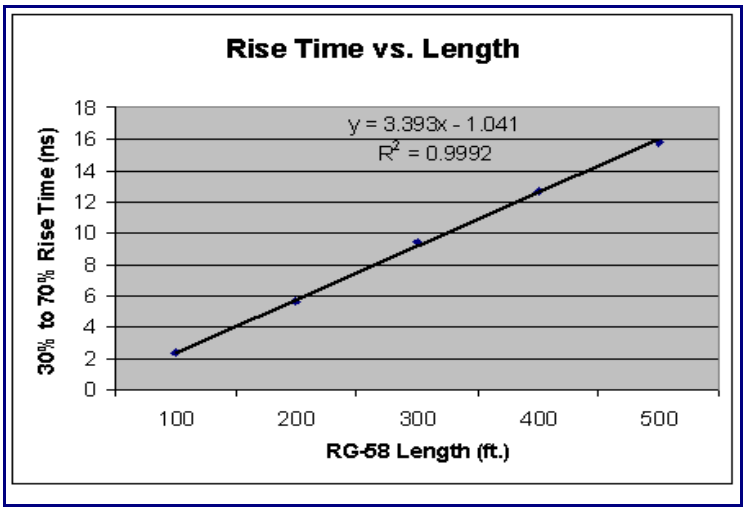

Figure 5.3: Rise Time vs. Length at 10%-90% and 30%-70%.[9]

---

[8] Table shows the tested properties of the various cables studied.

Endnotes continued on the next page

For each cable, the amplitude and the signal transit time through the cable were measured. From these parameters, the speed of the signal through the

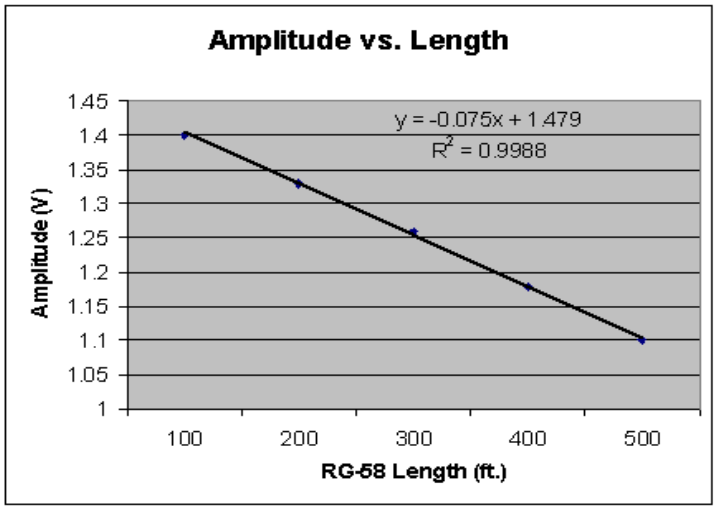

Figure 5.4: Amplitude vs. Length for RG-58 cable[10].

cables were determined. Our choice of cable for delay was the RG-58. Using this particular cable, lengths were varied from 100ft to 500ft and the resulting rise time and amplitude versus the lengths of the cable were measured.

[9] Figures show 10% to 90% and 30% to 70% of RG-58 cable rise time versus the cable length. The rise times are in nanoseconds (ns) and the length is in feet (ft).

[10] Figures show RG-58 cable amplitude versus the cable length. The amplitude is in volts (V) and the length is in feet (ft).

CHAPTER 6: DISCRIMINATOR TESTS

Discriminators are a useful tool in fast-timing applications and measurements. The main advantages of discriminator logic units are to count narrow pulses at very high rates, and to earmark the arrival time of these pulses. The standard design for the discriminator unit is to work with negative pulses from the anode of the photomultiplier tube being directly passed through a properly terminated 50Ω coaxial cable. The analog input pulses that satisfy the threshold of the discriminator are converted to logic pulses at the output of the timing discriminator. Thus these pulses can then be processed by a counter or TDC.

Our prototype goal is to achieve the best time resolution possible. For this reason we must utilize the most adequate discriminator within our electronic chain of modules. To carry out this utilization, we compared the operation and efficiency of the Leading Edge Discriminator (LED) versus the Constant Fraction Discriminator (CFD). Both these logic units accomplish the conversion of analog signals to digital signals, but they meet this task by two separate means. The LED generates a logic signal on the “leading edge” of the analog pulse signal that passes the pre-set threshold. This, however, potentially incorporates problems into the timing. If the rise time of the analog pulse of the discriminator

remains the same but the amplitude has changed, a shift or “walk” of the measured time occurs. This “time-walk” as it is called, comes about when you have two pulses that have the same rise time and different amplitudes. The pulse with the smaller amplitude will cross the LED threshold at a later time because the rise times are the same. Thus, this change in amplitude shifts the timing of the output digital signal by an amount that depends on the amplitude change. Therefore, the timing must be corrected for time walk when utilizing an LED.

For the CFD, these timing problems are not inherited by the module in that it compares a constant fraction of the analog signal and the signal itself to determine precisely the timing of the output digital signal relative to the input signal. The CFD splits the input signal and attenuates one part to a certain fraction of the original amplitude. It then inverts and delays the other part of the signal before both are summed together. After the attenuated part and the inverted-delayed part are added together, the zero crossing will give the time of the output signal created by the CFD. Herein lies the need to perform tests on both logic units to decipher the greatest productivity between them.

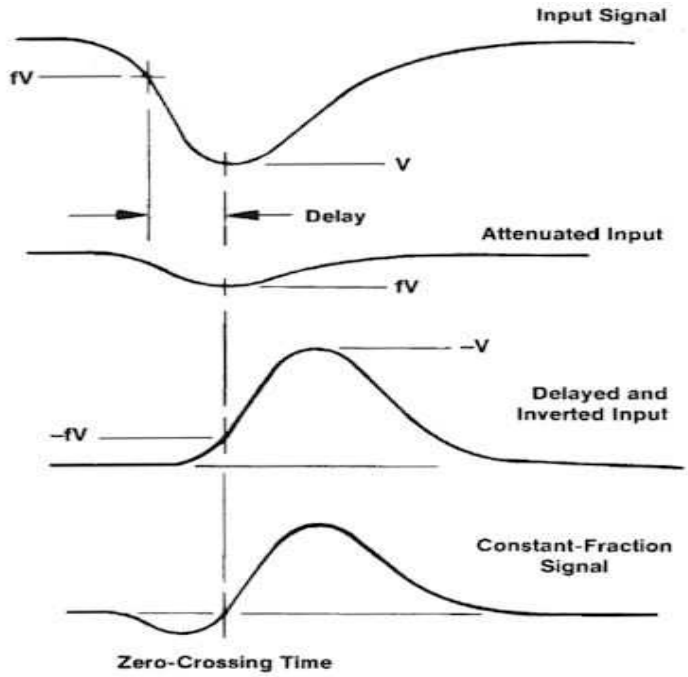

Figure 6.1: CFD Signal Behavior[11].

The CFD was analyzed to judge the best utilization method for the unit. The testing method consisted of using three pulse attenuators separate from the internal attenuation in the module, to witness the signals behavior.

[11] The Diagram shows the original pulse is delayed, inverted and added to an attenuated copy of the prompt pulses

.

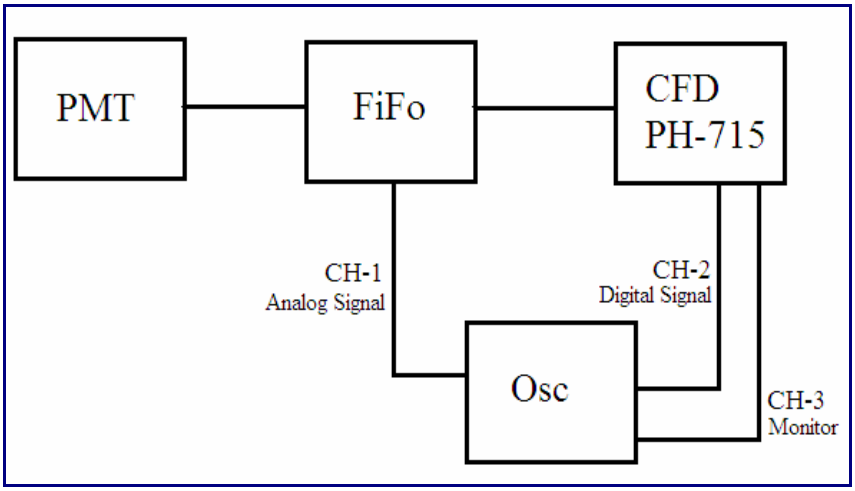

Figure 6.2: CFD Signal Schematic[12].

For effective testing, the delay of the signal produced by the external attenuator had to be measured and corrected appropriately.

[12] The Diagram shows the method for producing Fig. 6.2.

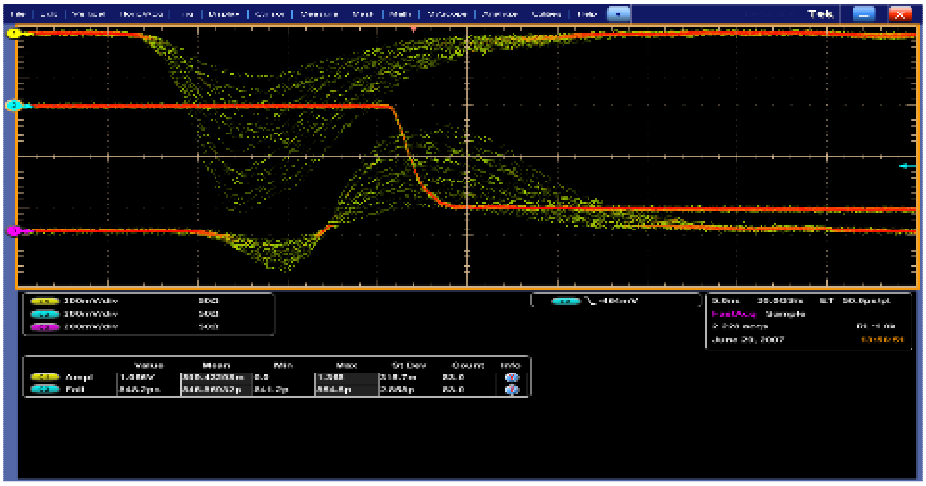

Figure 6.3: Constant Fraction Discriminator image from oscilloscope[13].

To find the additional external delay values, the measurements were taken without and with all utilized external attenuator combinations.

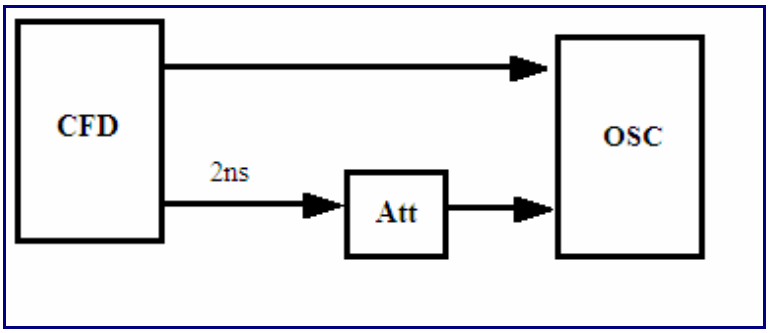

Figure 6.4: Constant Fraction Discriminator Attenuation Schematic[14].

[13] The image shows the signal that goes directly to the scope from the logic fan in/out, then the signal after passing through the logic fan in/out and the leading-edge discriminator (LED), and the signal after passing through the logic fan in/out and the constant fraction discriminator (CFD). This image shows how the CFD splits the analog signal to attenuate half and invert and delay the other half to find the zero crossing.

Endnotes continued on the next page

An additional, 2ns cable was added to connect the attenuators appropriately. This method utilized different attenuator combinations to find the best internal delay to optimize the CFD.

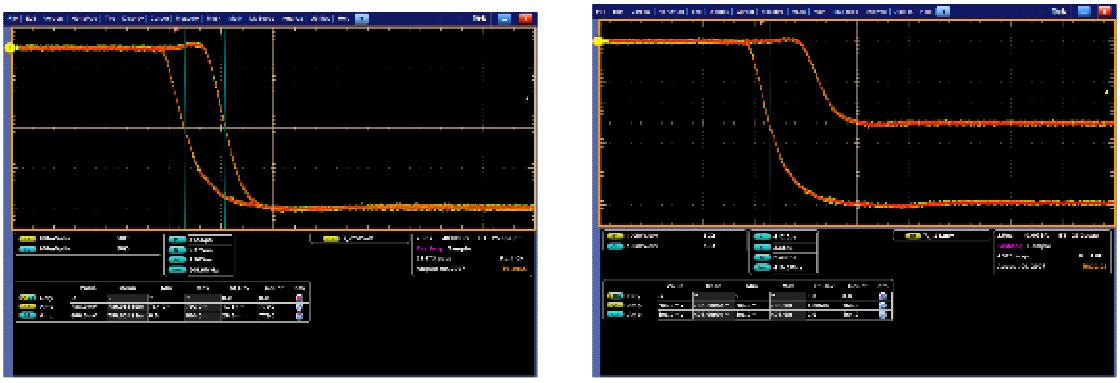

Figure 6.5: CFD external Attenuation Image[15].

Measurements for various time delays up to 15ns were performed. It was concluded that above 15ns, the data is no longer meaningful because it exceeds the signal width itself. Data was taken for several internal time delays in the CFD and the histograms were corrected to each external delay time. Once all histograms for each internal delay were plotted, they were added together to obtain an overall root mean square (RMS). We utilized this information to plot the RMS versus the internal delay.

---

[14] The Diagram shows the constant fraction discriminator (CFD) internal attenuation tests process. Two signals pass through the CFD where one goes directly into the oscilloscope, while the other is attenuated externally and then sent to the scope.

[15]Image shows the oscilloscope results of diagram 5.3. We clearly see the first signal fall and then the external attenuated fall a time later corresponding to the attenuated length.

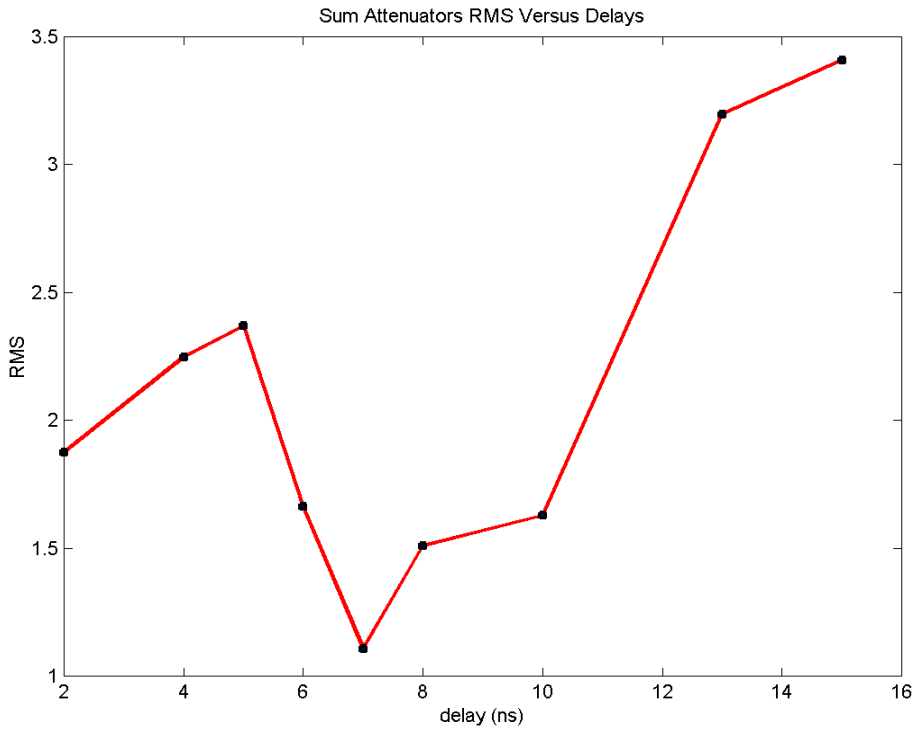

Figure 6.6: RMS vs. Delay[16].

Fig. 6.5 shows the overall optimized internal delay for producing excellent results using the CFD. From Fig. 6.6, we conclude that a 7ns delay is the optimal time delay for using the CFD.

[16] The plot shows the root mean square of the constant fraction discriminator (CFD) time delay histograms versus the delays in time. The results show that 7ns would be our optimized time delay for the CFD.

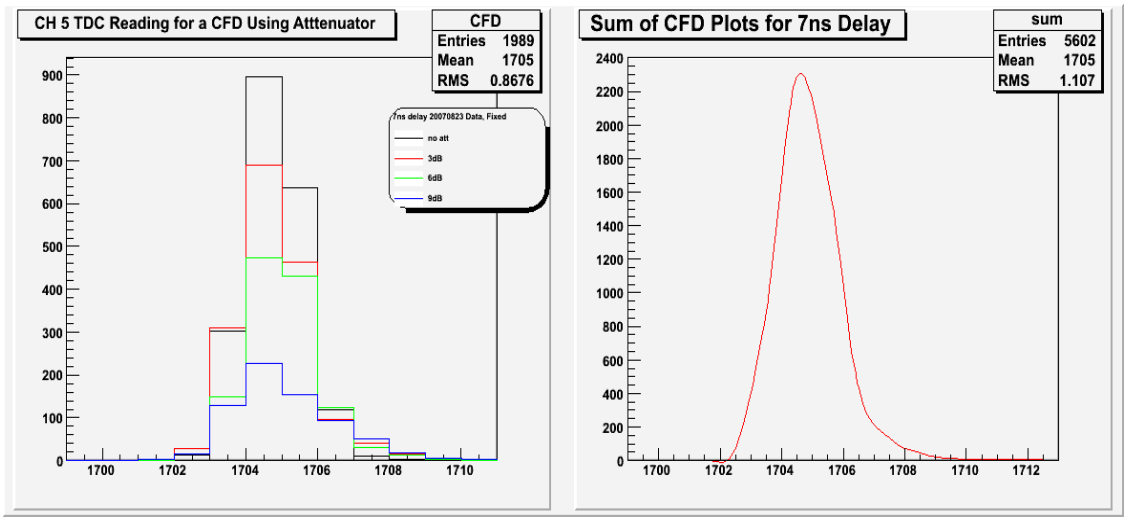

Figure 6.7: Various CFD Attenuations and Optimized CFD Delay plots[17].

[17] The left plot shows the different constant fraction discriminator (CFD) delays using an attenuator. For no attenuation (black curve), attenuation at 3 decibals (db) (red curve), attenuation at 6 db (green curve), and attenuation at 9 db (blue curve). Right plot shows the delays summed for a 7ns delay.

CHAPTER 7: TDC CALIBRATION & LINEARITY TESTS

Once the timing system has been chosen and incorporated, calibrating the system must take place. The TDC directly digitizes the time interval between start and stop pulses by using it to gate the output of a constant frequency clock. This method is limited to a frequency which corresponds to a period of 25ns. Thus, time intervals of several nanoseconds can be measured to an accurate level.

In calibrating the timing system and the absolute time width of each interval, a simple method to accomplish this task is using single source pulse to drive the start and stop channels. The output signal is separated into two signals where one leads into the start and the other into a stop after passing through a variable but well defined delay. This gives rise to the production of peaks in the TDC representing the different delays of cable. ***Knoll G., 1979*** [5] states that the distance between peaks produced by the different delays then gives a calibration of the time scale. This alludes to the path b) of Figure 7.1. The TDC calibration process involves mapping each TDC code to a specific time width by merging the results of full and discrete spectrum time interval measurements as described in the TDC Linearity pages. The following diagram illustrates the process from which the module/channel-specific calibration is derived:

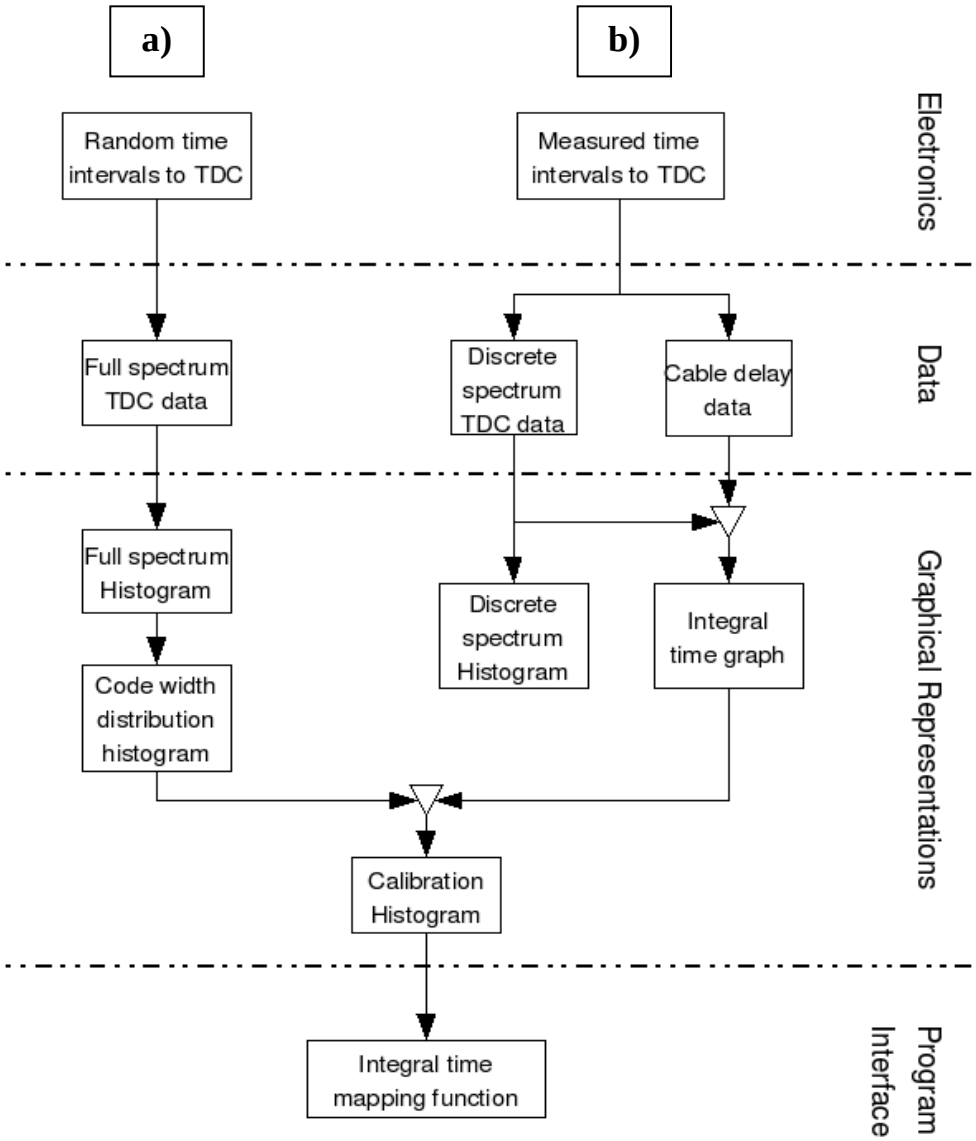

Figure 7.1: TDC Calibration Derivation[18].

[18] The following diagram illustrates the process from which the module/channel-specific calibration derives.

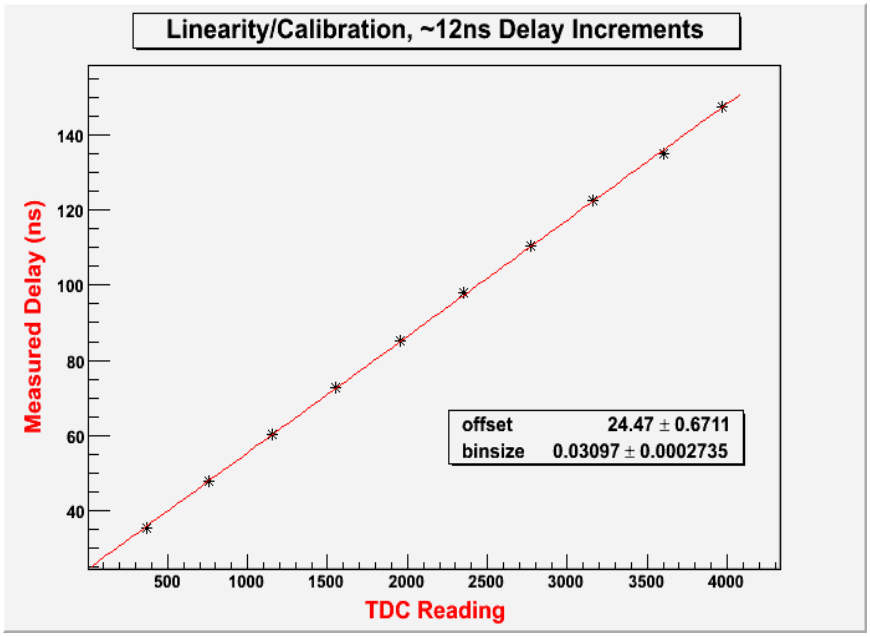

Figure 7.2: Delay vs. TDC Reading[19].

Another important aspect of the TDC measurement is its linearity. "In order to measure the linearity of the system, a source of random events uniformly distributed in time is necessary" ***Knoll G., 1979*** [5]. A sophisticated approach would be to utilize a random pulse generator, but we instead took advantage of the simplicity in using a radioactive source to produce pulses from our scintillator to phototube assembly. This method is shown in section a) of Figure 7.1.

[19] The Diagram shows the measured delay in increments of 12ns with respect to the time-to-digital (TDC) reading for each delayed increment. Plot displays the linearity of the TDC.

Our focus was to measure the differential non-linearity (DNL) profile of the TDC module, and then gain the overall linearity from this result. In our measurement, we tested a Phillips and Caen TDC CAMAC module. The procedures for the test were to feed a random start signal and a periodic stop signal in the TDC.

Figure 7.3: Differential Non-linearity (DNL) test conceptual schematic[20].

The start signal arrives randomly where the stop signal, with equal probability, arrived in a fixed-width time interval.

We placed a strontium radioactive source (Sr-90) on a Bicron scintillator with a PMT attached to it. The source provided random signals that passed through an LED to convert the signal to Nuclear Instrumentation Measurements (NIM) logic signals to be utilized for the timing. Once the data acquisition system (DAQ) was ready, a signal was sent for a common start of the TDC. In conjunction with the start, a timing unit (Phillips 794) with a period greater than the full range of the

[20] The Diagram shows a random signal being fed as a START for the time-to-digital (TDC) channel. Then sending a STOP signal that is sent to the TDC periodically.

TDC, provided a logic STOP pulse. Flowing through a logical fan in/out, the periodic stop signal was fed to all the TDC channels.

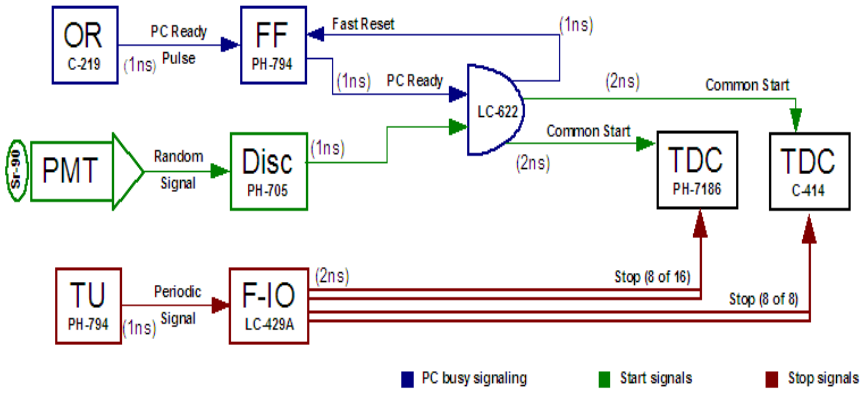

Figure 7.4: Realization schematic of conceptual approach[21].

What we expected was a uniform distribution of counts per time interval, being each bin, after measuring a large number of events. "The time intervals thus produced are uniformly distributed on the time scale and, with in statistical errors, should produce the same number of counts in each channel." Any deviation from the uniform distribution would represent a DNL of the TDC module.

[21] The Diagram shows the real electronic scheme the signals followed in the DNL measurement. OR refers to the output register unit, FF refers to logical fan in/out, PMT is the photomultiplier tube, DISC is the leading-edge discriminator, TU is the timing unit, F-IO refers again to logical fan in/out, and TDC is the time-to-digital converter unit.

For the Caen TDC, we found that it does not satisfy the DNL specifications that were documented by the company. It called for DNL specifications of less than 1.5% over a range beginning at 804 bins (20ns) and concluding at a maximum of 3780 bins. The documented Caen range corresponds to 75ns, but a peak around bin 1100 produced on 7 out of 8 channels reduced this range to 60ns. The expected and produced DNL values are shown in Fig 7.5.

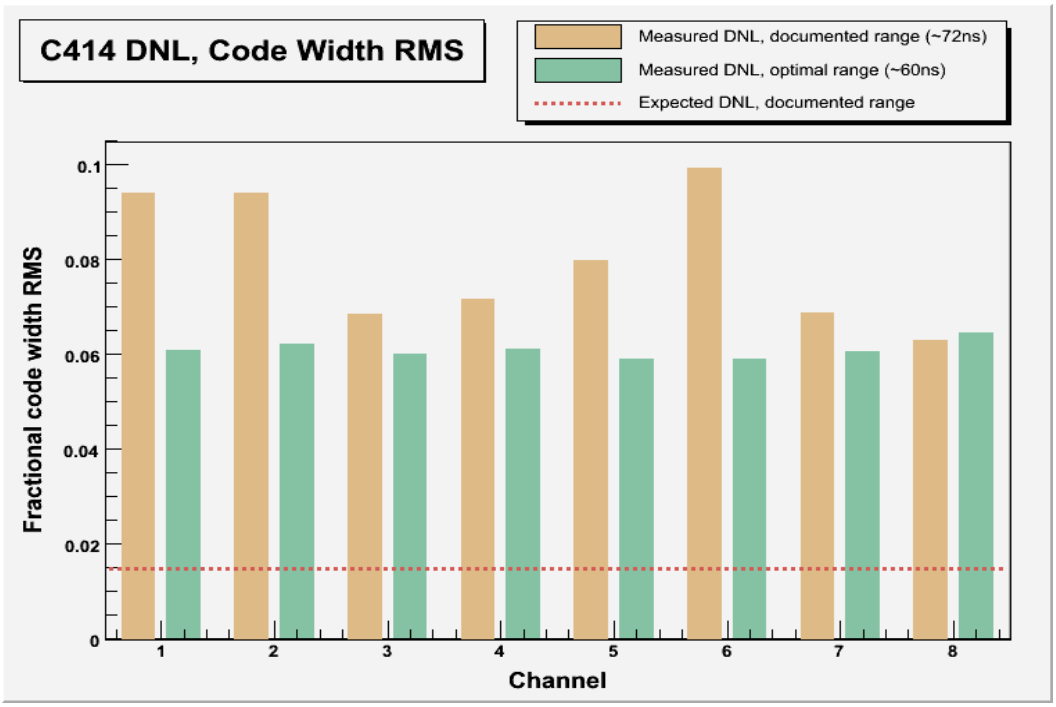

Figure 7.5: RMS of code width compared to their documented widths[22].

[22] The Diagram shows the measured documented ranges (brown bars) of the time-to-digital converter code widths compared to their optimal ranges 9green bars), and then the expected value (red line) shown as well.

Compared to the C414 TDC, the PH7186 has more consistent DNL over the full range, so the following table only includes additional ranges when the code width deviations are greatest near the beginning or end of the full range. Phillips Scientific's DNL metric, maximum deviation with respect to full range, has also been added for comparison to the company's document DNL specification, which claims a DNL of less than .015%.

CHAPTER 8: Time Resolution Tests

In high energy physics experiments, particle identification is accomplished through time-of-flight (TOF) measurements. The TOF system contains two important factors significant to its performance, the timing resolution and the efficiency of registering a good event. The overall goal for the existing forward TOF detector at CLAS is to improve the timing resolution. The current time resolution gives σ= 120 ps, and the upgrade calls for a resolution achievement of σ = 60ps.

Such an improvement of the resolution would allow the separation of pions from kaons up to a momentum of 3 GeV/c and pions from protons up to 6 GeV/c in momentum.

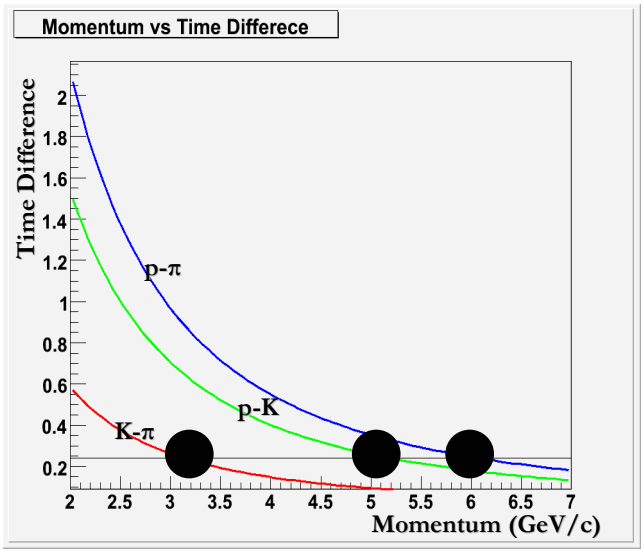

Figure 8.1: Time Difference versus Momentum of particles[23].

From Fig. 8.1, we can see that these particle separations assume a time difference of 4σ between the two particles. Thus, allowing a signal with ten times higher rates to be identified in the presence of other particles.

Previous prototypes using scintillation counters 200cm in length have produced resolutions of 70ps and 50ps. The 70ps resolution was accomplished using a single plane of scintillators, while the 50ps measurement was achieved by utilizing two scintillator planes ***Smith E., 1999*** [6].

[23] The Diagram shows the time difference versus the momentum of pion with kaon (red curve) and proton (blue curve). Also for proton and Kaon (green curve). Plot indicates the separation energies that can be achieved.

Both measurements were performed with fast scintillation and XP2020 PMTs. These resolution values are very encouraging to the upgrade goal of CLAS, the new design for the forward detector will leave the existing scintillation detectors in place and simply add an additional layer in front of it. This design should help to produce an overall resolution of 60ps utilizing two scintillation planes. Therefore, to ensure an adequate prototype resolution we tested different methods in search of the best resolution values achievable.

In TOF systems, there are three separate methods one can perform to test the time resolution of the system. These are the three identical counter method, reference counter method, and the source method.

8.1) THREE COUNTER METHOD

The commonly used method of measuring time resolution is the three scintillation counter method. This method is based upon precisely measuring cosmic ray particles' time-of-flight. The setup incorporates three identical counters equidistant of one another.

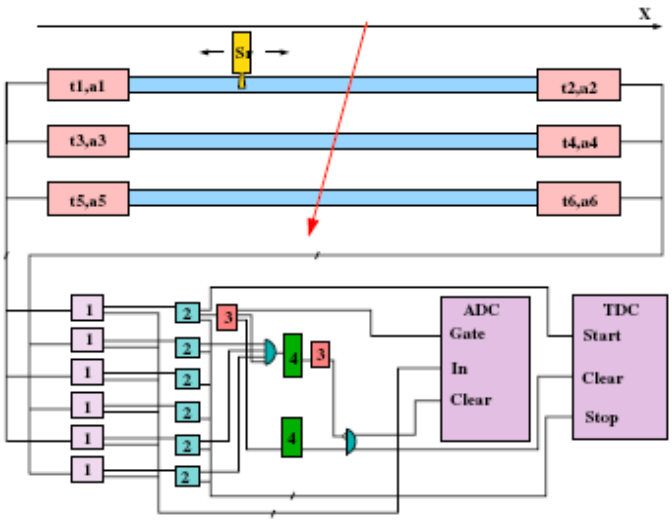

Figure 8.2: Schematic of 3 Counter Method[24].

The instant light flashes, the time follows the relation in Fig. 8.2

$$t_u = \frac{1}{2}(t_1 + t_2); t_m = \frac{1}{2}(t_3 + t_5); t_d = \frac{1}{2}(t_5 + t_6), \quad (1)$$

where t_i = 1,…,6 are the corresponding values from the TDC readout. It must also be taken into account that the $t_{u,m,d}$ values are expected to be independent upon the scintillator coordinates.

The procedure follows as cosmic particles of constant velocity (speed of light) strike the three counters which are equidistant and parallel to one another. From this interaction eq (2) is derived, that is independent of the position and angle.

[24] Schematic shows the 3 Counter Method setup with three identical counters with photomultiplier tubes attached, then the signal following the electronic chain to the analog-to-digital converter and time-to-digital converter.

$$t_{umd} = t_m - \frac{1}{2}(t_u + t_d) = 0 \quad (2)$$

This time parameter is smeared around zero due to the fact that the actual values are smeared by the time resolution. Thus, the method is based on the statistical analysis of eq. (2) residuals. Therefore,

$$\delta(t_{umd}) = \frac{1}{4}(\delta t_1 + \delta t_2) - \frac{1}{2}(\delta t_3 + \delta t_4) + \frac{1}{4}(\delta t_5 + \delta t_6) \quad (3)$$

And

$$\langle(\delta t_{umd})^2\rangle = \frac{3}{4}\langle(\delta t_i)^2\rangle = \frac{3}{4}\sigma^2_{PMT} \quad (4)$$

where *i* = 1,…,6 assuming all PMTs have timing properties that are the same. Thus, σ_{PMT} must be $\sqrt{\frac{4}{3}}$ times the standard deviation measured ***CHEN E., 2003*** [2].

This method is the typical one performed in time resolution and one we will ultimately utilize. However to cover all possible avenues of timing measurements, we performed tests using two other methods to gauge how good our results would be from non-standard means. Keep in mind the measurements have not been done to date in our prototype measurements. The intent of this section is simply to apprise you of the normal means utilized. Seemingly, there are no results to be shown but the overall concept of the method is understood.

8.2) REFERENCE COUNTERS METHOD

This method involves three scintillators where two are thin counters and one is a long extended counter. The two short counters are used as reference counters and the longer counter is the actual test counter. The time resolution is measured by using cosmic rays passing through all three counters. All counters have PMTs on each end and are positioned so that the test counter is in the middle of the reference counters.

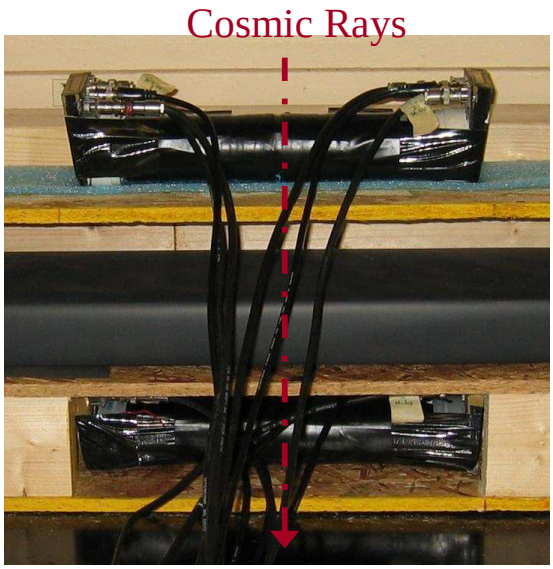

Figure 8.3: Reference Counter Method Image[25].

[25] Image shows the experimental setup of the Reference Counter Method, where we have to short counters for reference and the long test counter in the middle.

The cosmic ray events are selected by the coincidence of the reference counters. Meaning, once an event in both counters coincide with one another, a good event signal is registered. The coincidence trigger pulse defines the TDC start time and generates an ADC gate.

The reference counters which are positioned next to the test counter provide a timed measurement of the cosmic ray passing through the test counter. This time is recorded for each event and this procedure is repeated for the desired amount of events.

The time measurement of the PMT must be time walk corrected, which simply accounts for the varying time needed for the pulse to exceed the discriminator threshold. The equation for the time walk is given in Eq. (5), where T_i is the

$$T_i' = T_i - a_i Q_i^{-b_i} \quad (5)$$

measured time of the TDC and Q_i the ADC count with the subtracted pedestal. The position dependent time distribution is defined for the left and tight PMTs as:

$$T_{\mathrm{L}}(z) \equiv T_3' - c_3 z - T_{\mathrm{ref+}} \quad (6)$$

$$T_{\mathrm{R}}(z) \equiv T_4' - c_4 z - T_{\mathrm{ref+}} \quad (7)$$

where c_{eff} is the effective propagation speed of light on the test counter. The constants a_i, and b_i, are found by minimizing the widths of the distributions. Both $T_L(z)$ and $T_R(z)$ contain the reference counters time distributions defined as:

$$T_{\text{ref}+} \equiv (T_1' + T_2')/2 \qquad T_{\text{ref}-} \equiv (T_1' - T_2')/2 \qquad (8)$$

Once we have the time distributions plotted from the recorded data, we fit these distributions to obtain the overall time resolution (σ_L, σ_R) for the left and right side of the test counter. These resolution values eqs. (9) and (10) are then utilized to gain the specific widths to calculate the total time resolution of the system.

$$\sigma_3(z) = \sqrt{\sigma_{\text{L}}^2(z) - \sigma_{\text{ref}}^2} \qquad (9)$$

$$\sigma_4(z) = \sqrt{\sigma_{\text{R}}^2(z) - \sigma_{\text{ref}}^2} \qquad (10)$$

And from these equations, the weighted average of the system time is given by:

$$T_{\text{system}}(z) \equiv \frac{T_{\text{L}}(z)\sigma_4^2(z) + T_{\text{R}}(z)\sigma_3^2(z)}{\sigma_3^2(z) + \sigma_4^2(z)} \qquad (11)$$

To gain the time resolution of the test counter, the reference counter contribution must be subtracted in quadrature giving a resolution equation of:

$$\sigma_{\text{tof}}(z) = \sqrt{\sigma_{\text{system}}^2(z) - \sigma_{\text{ref}}^2} \qquad (12)$$

This method helped in covering a possible avenue to time resolution measurements other than the standard method, but it proved to be unproductive by taking an excessive amount of time to produce events during testing. The event rate was of the order of 1 event per 10 minutes.

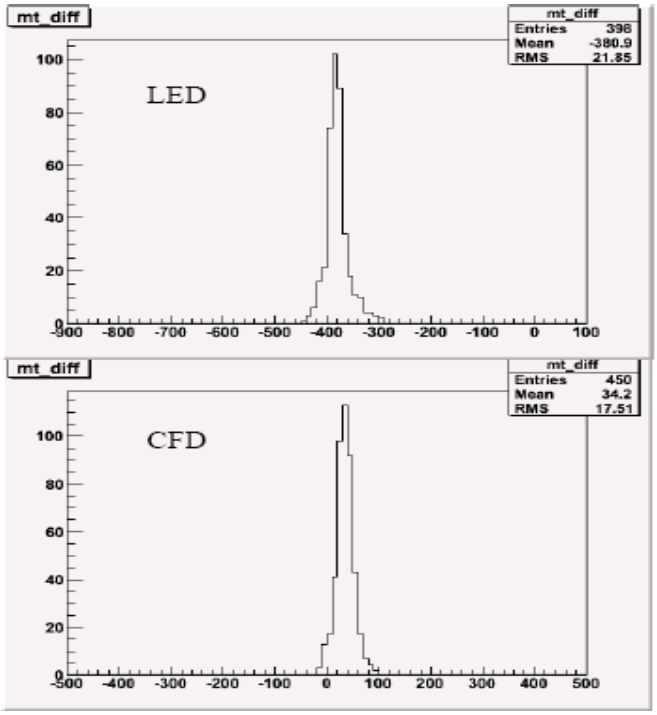

Figure 8.4: LED and CFD results of Reference Method[26].

This difference of the left and right times was taken and fit to extract the channel width. Then an overall σ = 390ps was calculated.

8.3) SOURCE METHOD

This method of measuring time resolution was adopted from Kyungpook National University [1], where they referred to it as the "coordinate method". It was

[26] The histograms show the time width distributions from the reference method for a LED being utilized and then for a CFD.

deemed this way simply because it takes into account the relation between coordinate x of the light flash and the signal arrival times for the left and right PMTs. This method we followed for our measurements, but will refer to it as the "source method" in that we only needed a scintillation bar and a radioactive source to complete all measurements.

Our setup consists of a scintillation bar of 213cm in length with EMI 9954B05 PMTs on both ends. From the PMT, the dynode signal is sent for an ADC gate, while the anode gives the TDC start signal. The anode signal passed through the electronic chain that required a high threshold and low threshold, but triggers an event on the high threshold and provides the timing on the low threshold. The high threshold is set to 700mV while the low is set to 200mV. Each threshold required a coincidence between right and left signals before a good event will be registered. Fig. 8.5 shows the schematic of the setup diagram.

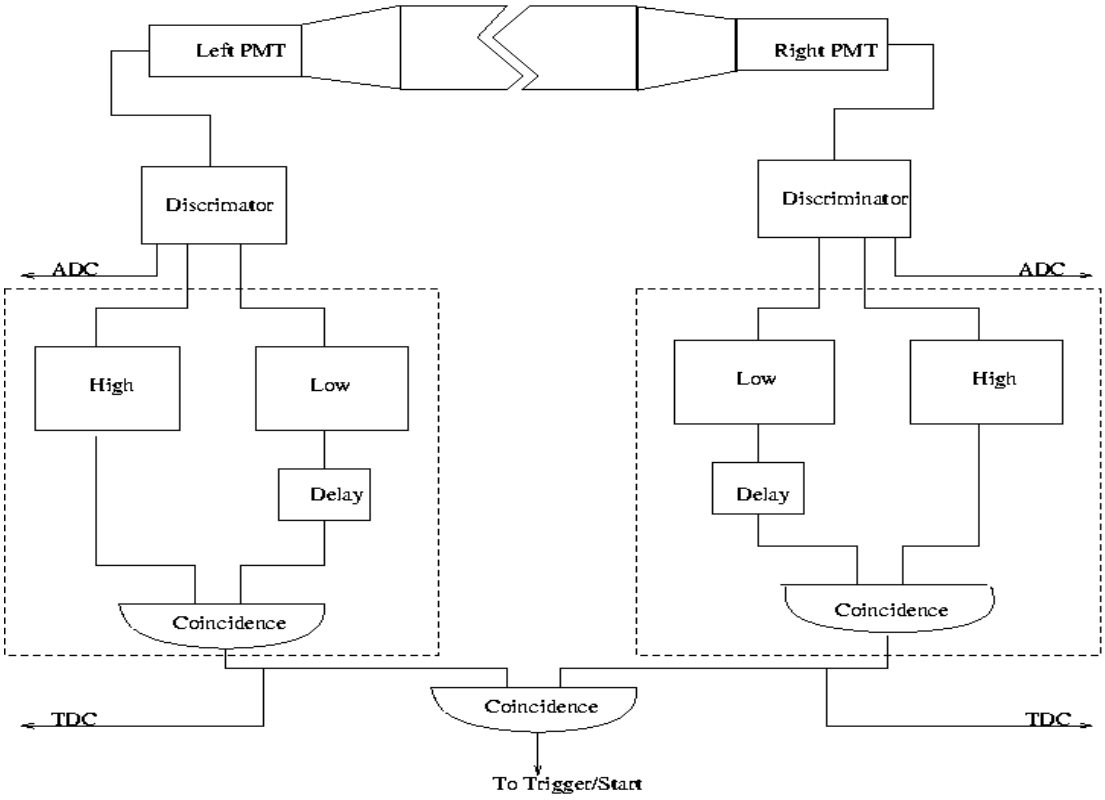

Figure 8.5: Schematic of Source Method[27].

The digitized value of the TDC was given by

$$t_x = t_l - t_r = \frac{2x}{c_s} + const, \quad (13)$$

[27] The Diagram shows the Source Method where a high threshold is demanded and the low threshold is triggered on. A coincidence between the left/right high thresholds and left/right low thresholds were required for a good event pulse.

where *x* is the coordinate of the light flash in, t_l is left PMT time, and t_r is the right PMT time. The standard deviation of t_x relates to right and left PMT resolutions by

$$\langle (\delta t_x)^2 \rangle = \langle (\delta t_l)^2 \rangle + \langle (\delta t_r)^2 \rangle + \langle (\delta t_{TDC})^2 \rangle + \left(\frac{2x}{c_s}\right)^2 \langle (\delta x)^2 \rangle \quad (14)$$

where $\langle (\delta t_{l,r})^2 \rangle$ are the standard deviation times for both PMTs, $\langle (\delta t_{TDC})^2 \rangle$ is the intrinsic resolution of the TDC, and $\langle (\delta x)^2 \rangle$ gives the size of the radiation source. The intrinsic resolution of the TDC was gathered during the TDC calibration and differential non-linearity tests. The Phillips TDC module used gave an intrinsic resolution range from 24ps to 26ps, depending on which input channel of the module that was used. To get the size of the source, the ionizing source had to be stepped across a PMT in 1mm steps using a lead window. We cut a small strip in the lead, to create a window where we moved the source in 1mm increments over the edge of the lead window. With this setup, the lead should restrict the source to zero count rate until it reaches the edge of the opening. Thus the rates in the open window should be higher than at the edges, and from the given count rate distribution we can obtain the size of the source. Fig. 8.6 displays the experimental setup and shows the distribution of count rate in millimeter steps.

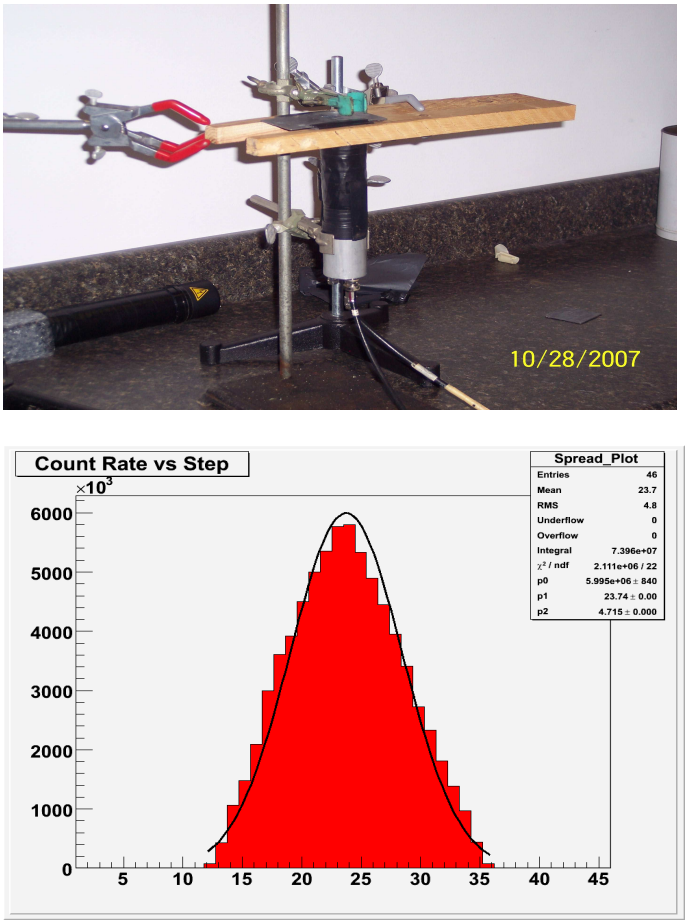

Figure 8.6: Beam spot setup and fitted distribution[28].

An ionization with a known coordinate can be provided by β-particles from the localized radioactive source. Seemingly, the single PMT resolution can be determined as

[28] The first image shows the experimental setup used to carryout the source size measurement, where you see a lead sheet with a small window cut into it over the surface of a PMT. The histogram shows the distribution from taking 1mm steps across the lead window and fitting the distribution to gain the size of the source.

$$\sigma_{PMT} = \frac{1}{\sqrt{2}}\sqrt{\langle(\delta t_x)^2\rangle - \langle(\delta t_{TDC})^2\rangle - \left(\frac{2x}{c_s}\right)^2 \langle(\delta x)^2\rangle} \qquad (15)$$

The first time resolution results gave σ = 650 ps.

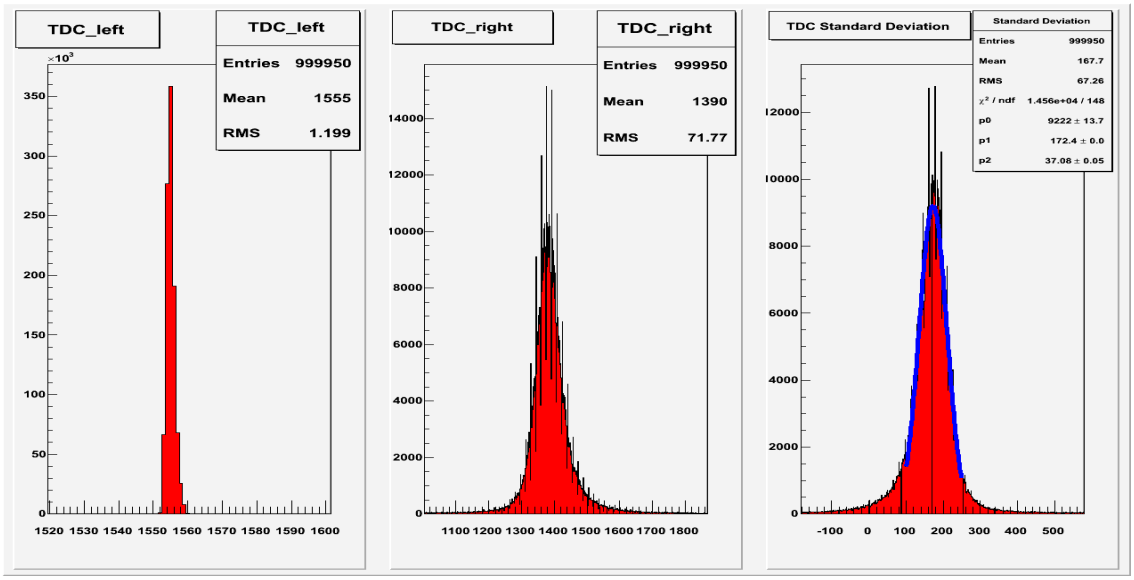

Figure 8.7: First time resolution results[29].

This was simply triggering on low threshold without the demand of high as well, and without any time-walk corrections applied to the collected data. The next measurements were performed by demanding high threshold but measuring the low to produce a better resolution. Fig. 8.7 shows our fitted results were the resolution improved to σ = 510 ps.

[29] The histogram shows the left TDC value used for timing, the right TDC value for the distribution over the bar, and the difference between left and right TDC values with a fit to find the width to calculate the time resolution.

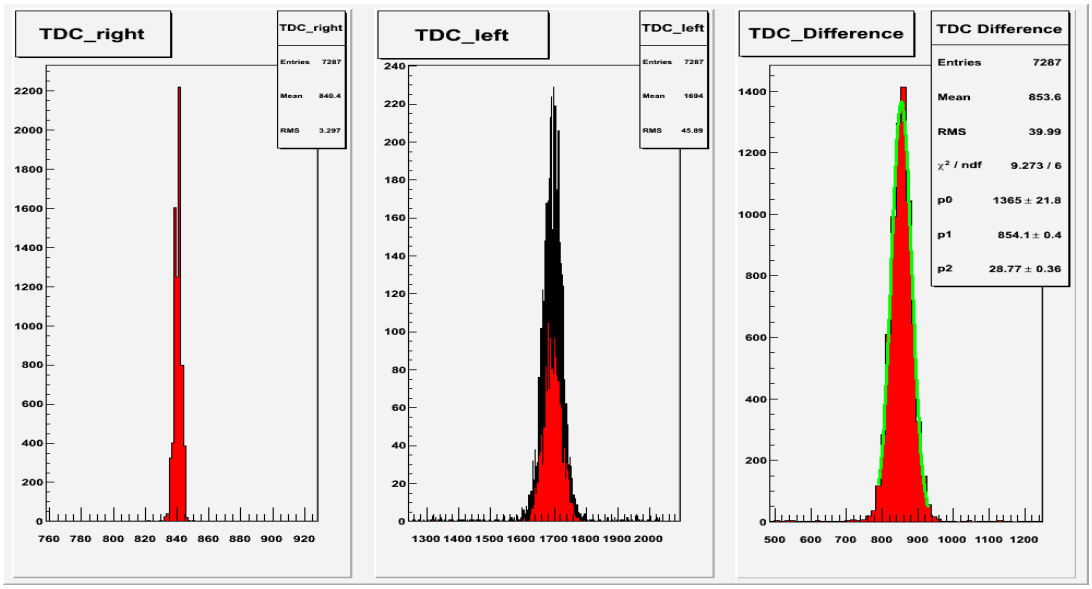

Figure 8.8: The second time resolution results[30].

To correct the time-walk introduced by the leading edge discriminators, we measure the ADC amplitude and the offset to be utilized in the correction equation. The ADC offset is accomplished by generating a random event that periodically trigger a read out. This offset is utilized in the correction equation, where it is subtracted from the ADC value.

The time walk contains a coefficient that is a fitted parameter given by Fig. 8.9. In this plot we look for the lowest value of sigma to find the best parameter to be used in the time-walk correction.

[30] The histogram shows the left TDC value used for timing, the right TDC value for the distribution over the bar, and the difference between left and right TDC values with a fit to find the width to calculate the time resolution. This time the concept of demanding a high threshold while triggering on the low threshold was used.

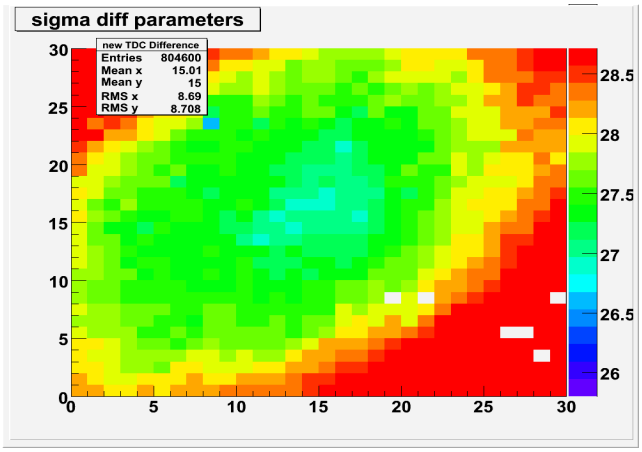

Figure 8.9: Time Walk Correction Parameterization[31]

From the plot, we find that the best (lowest) sigma produced is around 14. Once time-walk was applied, our new time resolution yielded σ = 470 ps.

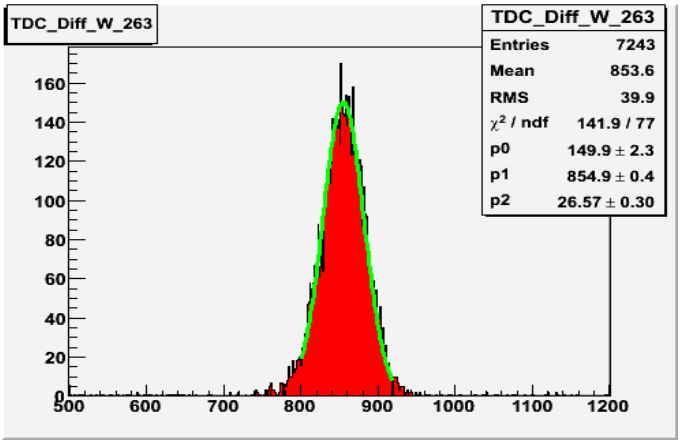

Figure 8.10: Best time resolution result[32]

[31] The histogram shows the fitted widths for left TDC with time walk correction plotted against those of the right TDC with time walk corrections. The plot shows us our best possible resolution widths with time walk correction.

[32] The plot shows the best time difference plot with time walk corrections.

CONCLUSION

The TOF upgrade at 12GeV, looks to extend the particle identification to higher momenta, better charged particle traveling time resolution, and improved two pion separation. It is our conclusion that with adequate electronic modules and optimized detector components such as PMTs and magnetic shielding, we will as optimized tools reach a time resolution of great improvement. With these three different methods, we are confident to produce the needed detectors with time resolutions that will definitely improve the existing CLAS time of flight resolution. We are still too early in our measurements to gauge the success of whether we will meet the overall resolution improvement by a factor of two. From the methods discussed in this thesis, we can conclude that the reference counter method is one that is not suitable to perform detector test series. The biggest problem that arises in this method is that it takes too great of time to produce an event using this method. Our best event time production for the reference method was about 10 to 15 minutes per event. The source method was by far the easiest method to carry out measurements. It did not provide the best expected results but will provide a prevalent comparison to the 3 counter method when it is performed.

One reason that the reference method produced a better resolution than the source method, is that it receives an energy deposit of around 10 MeV. The source method in comparison obtains about 1 MeV of deposited energy which means a greater number of photoelectrons cascade within the PMT for signal production. Another problem to resolve that leads for both methods to lower resolution results would be the overall concurrent condition of the scintillators, light guides and PMTs. The scintillator bar that we used was previously constructed at Jefferson Lab and had several defects, such as improper gluing, insufficient wrapping, defective phototubes, and misalignment of the light guide to scintillation. All these parameters will have to be optimized to for an improved study of the time resolution.

LIST OF REFERENCES

[1] Batourine, V. N., Kim W., Nekrasov D. M., Park K., Shin B., Smith E. S., and Stepanyan S. S., “Measurements of PMT time resolution at Kungpook National University”, CLAS-NOTE, 2004-016, May 2004.

[2] Chen E., Saulnier M., Sun W., and Yamamoto H., “Tests of a High Resolution Time of Flight System Based on Long and Narrow Scintillator”, Volume 1, 6, 2967-2974, August 2003.

[3] Eichholz G. G., Poston J. W., “Principles of Nuclear Radiation Detection”, Ann Arbor Science Publishers, Ann Arbor, 1979.

[4] Grupen C., “Particle Detectors”, Cambridge University Press, New York, 1996.

[5] Knoll, G. F., “Radiation Detection and Measurement”, John Wiley & Sons, Inc., 1979.

[6] Smith, E. S., Carstens, T., “The time-of-flight system for CLAS”, NIM. A 432, 265–298, 1999.

[7] Abbott, D., Avakian, H., et.al. “The Hall B 12 GeV Upgrade”. 112, 227–237, 2002.

[8] Photomultiplier Tubes Catalog. “Photonis Imaging Sensors”. A-5,2004.